Semi-continuous approach for the modeling of thin woven composite panels applied to oblique impacts on helicopter blades

Pablo Navarro, Aubry Julien, Steven Marguet, Jean-François Ferrero, Sandrine Lemaire, Patrice Rauch

Semi-continuous approach for the modeling of thin woven composite panels applied to oblique impacts on helicopter blades

P. Navarro [a], J. Aubry [a], S. Marguet [b], J.-F. Ferrero [b,*], S. Lemaire [c], P. Rauch [c]

[a] *Université de Toulouse/ICA/ISAE, 10 av. E. Belin, 31055 Toulouse Cedex, France*
[b] *Université de Toulouse/ICA/UPS, 118 Rte de Narbonne, 31062 Toulouse, France*
[c] *Eurocopter Marignane/BDD – Aéroport Marseille P., 13725 Marignane, France*

In aeronautics, passenger safety and reliability of structures are essential aspects. In the specific case of helicopters, blades are subjected to impact loadings. Modeling these phenomena continue to be difficult and experimental tests often replace the prediction. The following work will focus on the experimental and numerical study of an oblique impact on the skin of the blade. It is equivalent in a first approach to an impact on a sandwich panel made up of a foam core and a thin woven composite skin. The objectives are to identify the mechanisms of damage in the skin for this kind of loading and to develop a representative modeling of the chronology of damage adapted to the modeling of the complete structure. Thus, a semi-continuous F.E. explicit modeling has been developed. It relies on the development of a specific damageable element at the bundles scale. Satisfactory numerical results are obtained. They allow the identification of the damage mechanism of the woven skin.

1. Introduction

In the field of transport, particularly in aeronautics, the slightest weakness in a part of the structure can have serious consequences. Helicopter blades are particularly sensitive to impact loading. Indeed, during flight, blades may be subjected to impacts with various soft or hard bodies such as birds or hailstone. The impact velocity can be up to several hundred meters per second. It is directly linked to the rotational speed of the blades. The complexity of these impacts is increased by the composition of the blades. A blade is made up of a main spar with unidirectional glass–epoxy composite in the leading edge; of a skin generally made of two or three plies of glass–epoxy and (or) carbon–epoxy woven fabrics; of a polyurethane foam core; of a glass–epoxy unidirectional composite trailing edge; and of a protection made of stainless steel that covers the leading edge. One or more composite carbon–epoxy ribs stabilize the skins. Two kinds of impact can be distinguished. The first one is a frontal impact on the leading edge. The second one, which is dealt with in this study, is an oblique impact on the lower surface of the blade (Fig. 1).

An oblique impact is characterized by the angle of incidence of impact, generally between 10° and 20°, caused by the inclination of the blade in flight. Given the geometry of the impacted area, this blade can be assimilated to a sandwich structure made up of a foam core and a skin built up of two plies of woven glass/epoxy composite.

Many experimental studies deal with the impact on laminate panels for which the mechanisms of damage can be described in three steps [1]. Chronologically, the damage of the matrix precedes delamination and failure of the fibers. Their relative influence depends mainly on the characteristics of the fibers, the resin, the stacking sequence and the applied loads [2–6]. Woven laminates have similar damage modes [7], but a chronological classification cannot be made as clearly as in the unidirectional laminate case. As for sandwich structures [8–10], the behaviors differ from those observed in laminated panels, due to both the low thickness of the skins and the presence of the core (foam or honeycomb) which stabilizes them. Many failure modes have been brought to light:

- compression failure of the upper skin,
- foam compression with a tensile failure of the lower skin,
- shear failure of the foam coupled with a buckling of the upper skin,
- shear failure of the foam coupled with a tensile failure of the lower skin.

As the impact velocity increases [11,12], the impact response becomes localized and shear is the main failure mode.

To reduce certification and development costs, the aircraft industry would like to use computational methods. This would enable them to predict structural integrity of composite structures

* Corresponding author. Tel.: +33 5 6155 8645; fax: +33 5 6155 8178.
E-mail address: Jean-Francois.Ferrero@isae.fr (J.-F. Ferrero).

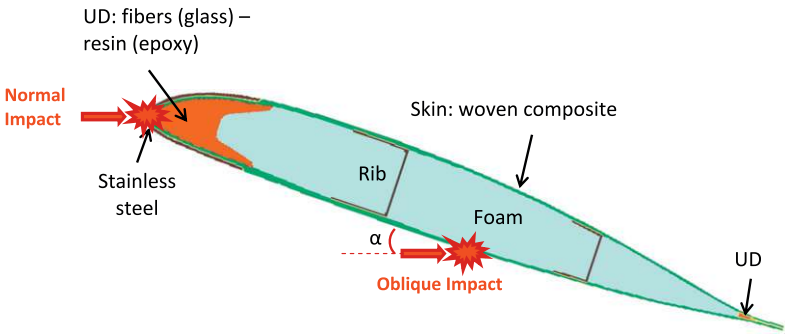

Fig. 1. Section of a blade and materials used. (For interpretation of the references to color in this figure legend, the reader is referred to the web version of this article.)

under impact from soft or hard bodies. The simulation of impacts on woven composite panels is performed using three major strategies. The first one consists of modeling the structure at the panel scale, using 2D elements and a homogenized orthotropic material law [13,14]. Damage parameters are introduced to represent the breakage of the warp and weft fibers, the failure of the bundles and the resin. These models are particularly efficient for ballistic impacts on woven plates. The second strategy consists of building models at a smaller scale to represent the details of the structure of a woven ply. In [15] the bundles are modeled with 3D solid elements in order to take into account the friction. In [16] the scale is lowered at the fiber scale. Each thread is modeled by a chain of rod elements and the contact taken into account. These models allow a good representation of the influence of the weaving, but for longer computing times. The third approach consists of finding a compromise between the two previous modeling scales. In [17], a representative pattern of the woven fabric is modeled with 3D solid elements. The whole woven panel is modeled at a larger scale and the calculation is conducted using a multi-scale method. This method allows the representation of the resin cracking, the resin/fiber interfacial debonding and the fiber breakage. Another multi-scale method is described in [18]. The fabric is represented at the bundle scale with 3D solid elements in the impacted area. Elsewhere, the fabric is modeled with 2D homogenized shell elements. Using this strategy, the calculation time is reduced five fold.

A numerical modeling of the thin woven skin based on experimental observations has been developed in this study. The model presented here uses an original scale: the woven mesh fabric scale. It allows a correct simulation of static indentations, low velocity normal impacts and high velocity oblique impacts. It also permits the identification of the damage scenario.

2. Experimental analysis

High velocity oblique impact tests have been performed in order to identify the chronology of the damage mechanisms for the thin woven composite skin. These tests have been carried out with an air gun. The impactor is a 19 mm diameter steel ball with a mass of 28 g. The core of the impacted panels is an aeronautical foam (Rohacell A51). The two skins are made up of two plies of glass/epoxy woven fabric (7781/913) prepregs oriented at 0–90° from the firing direction. Special attention has been taken to balance the proportions of warp and weft fibers in each direction. The composite skin thickness is 0.7 mm. The material characteristics are given in Table 1.

The specimens are square, 200 mm on each edge, and 20 mm thick. The sample is placed on a table tilted at 15° from the impact axis (Fig. 2). This value has been chosen to reproduce the flight conditions of the helicopter blade. The impact velocity has been

Table 1
Characteristics of the materials.

Woven fabric (7781/913)		Foam (Rohacell A51)	
Density (kg/m^3)	1900	Density (kg/m^3)	52
Elastic modulus (MPa) $E_x = E_y$	17,000	Elastic modulus (MPa)	70
Shear modulus (MPa)	3000	Shear modulus (MPa)	19
Poisson ratio	0.13	Compressive strength (MPa)	0.9
Tensile strain limit	0.025	Tensile strength (MPa)	1.9

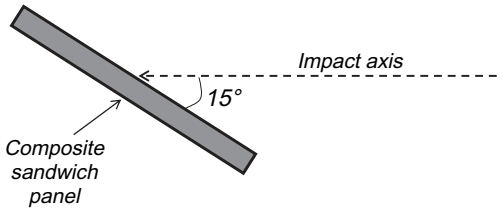

Fig. 2. Presentation of the oblique impact tests.

varied from 60 m/s to 130 m/s, which corresponds to impact energies evolving from 50 J to 230 J.

These tests allow the observation of two states of damage to the woven skin depending on the impact energy (Fig. 3).

The first state of damage is observed under lower impact energies. Micro-cracking of the resin is visible using a scanning electron microscope. However, no failure of the bundles is observed. The impactor rebounds during the impact. The second level of damage, obtained under greater impact energies, is characterized by the damage of the resin and the breakage of fibers. For these energies, the impactor either rebounds or perforates the skin. If the steel ball rebounds, the resulting fracture surface is a longitudinal crack oriented along the firing axis. For a given configuration of the sample, the threshold between these different states of the skin depends on the impact angle and on the mass and velocity of the impactor.

Furthermore, the analysis of the tests' results brings to light the mechanisms of damage of the thin woven composite skin (Fig. 4). Firstly, the damage of the skins begins with the apparition of micro-cracking in the matrix resin. Then, once the resin is totally damaged, the bundles, which are no longer stabilized, carry the whole load. Finally, if the strain in the fibers reaches the ultimate tensile strain, the fibers break and the skin tears. As the skin is made up of 2 woven composite layers, no delamination is observed.

In order to optimize the oblique impact response of a helicopter blade, a study of the influence of the various parameters (materials and impact conditions) on the amount of damage must be carried out. Therefore, a numerical modeling has been developed.

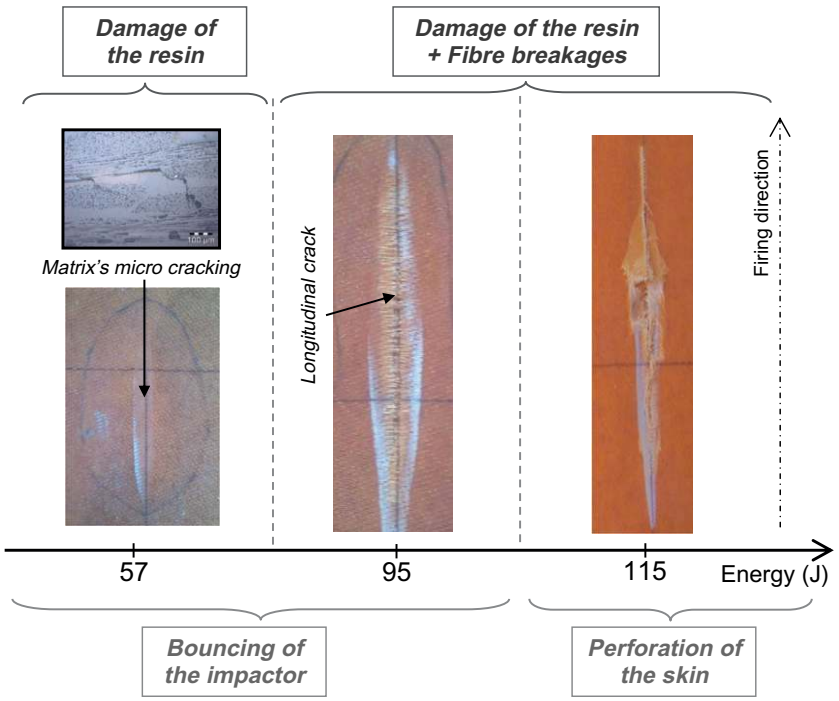

Fig. 3. Influence of the impact energy on the damage of the skin. (For interpretation of the references to color in this figure legend, the reader is referred to the web version of this article.)

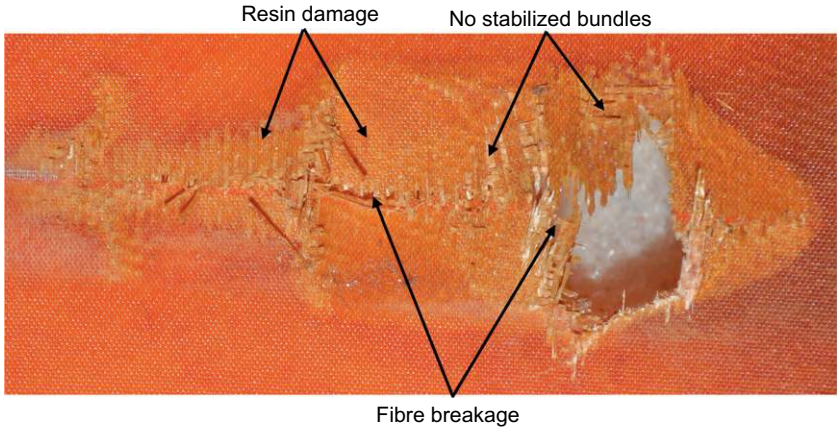

Fig. 4. Damage mechanisms of the woven skin. (For interpretation of the references to color in this figure legend, the reader is referred to the web version of this article.)

3. Modeling presentation

3.1. Principle

In light of previous observations, a semi-continuous modeling for the thin woven composite blade skin has been suggested. It relies on the chronology identified experimentally. The idea is to build a modeling which can represent the behavior of the undamaged woven skin (a continuous panel) as well as that of the damaged skin (non-stabilized bundles). Therefore, the modeling has been developed at the woven fabric mesh scale. As a consequence of the same warp and weft distribution, no distinction has been made between the modeling of the two membrane directions. As delamination is not predominant, only one element is taken through the thickness. The bundles are represented by the use of 1D rod elements. This truss structure is stabilized by a damageable 2D element, which has been fully developed (Fig. 5).

The plate theory gives the normal forces per unit length (vector N) and the bending moments per unit length (vector M) of the woven skin. They are obtained from the membrane and bending strains (respectively vectors ε and k) by the introduction of three constitutive matrices A, B and C (1):

$$\begin{Bmatrix} N \\ M \end{Bmatrix} = \begin{bmatrix} A & B \\ B^t & C \end{bmatrix} \begin{Bmatrix} \varepsilon \\ k \end{Bmatrix}$$
$$\text{with} \quad N = \begin{Bmatrix} N_{xx} \\ N_{yy} \\ N_{xy} \end{Bmatrix}, M = \begin{Bmatrix} M_{xx} \\ M_{yy} \\ M_{xy} \end{Bmatrix}, \varepsilon = \begin{Bmatrix} \varepsilon_{xx} \\ \varepsilon_{yy} \\ \varepsilon_{xy} \end{Bmatrix}, k = \begin{Bmatrix} k_{xx} \\ k_{yy} \\ k_{xy} \end{Bmatrix} \quad (1)$$

A is the constitutive matrix of the membrane behavior and C the constitutive matrix of the bending behavior. B represents the membrane-bending coupling. In this study the skin is a balanced woven laminate, so that $B = 0$.

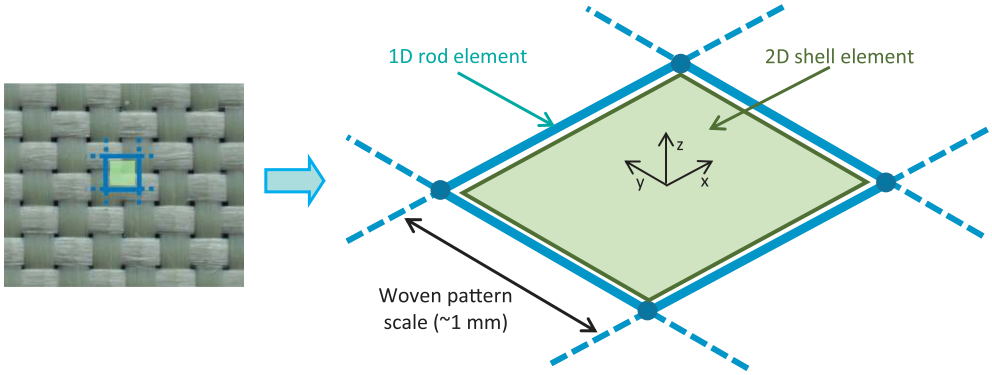

Fig. 5. Modeling principle. (For interpretation of the references to color in this figure legend, the reader is referred to the web version of this article.)

For the membrane loading, the stiffness of the woven skin is represented by both the rods and the 2D shell elements. However, for the bending and transverse shear loading, the rods do not have any influence (2):

$$\begin{aligned} A &= A_{shell} + A_{rod} \\ C &= C_{shell} \end{aligned} \tag{2}$$

where A_{shell} and C_{shell} are respectively the constitutive matrix of the membrane behavior and the bending behavior of the 2D shell element. A_{rod} is the stiffness of the rod elements. The matrix A_{shell} represents the stiffness of the resin. The matrix C_{shell} represents the stiffness of the whole skin. The damage mechanisms (micro-cracking of the resin between and inside the bundles) are taken into account by damaging the matrices A_{shell} and C_{shell}.

The connection between the 1D and 2D elements is made at the nodes. The interaction between the bundles and the resin is neglected.

3.2. Formulation

The specific shell element has been developed from Belytschko's formulation [19]. It is based on the theory of bending of shells. To increase stability and to avoid hourglass strain modes, the element incorporates four integration points. As this 2D element is considered as homogenous in the thickness direction, the transverse shear strain has been calculated using Hencky-Mindlin's theory. The membrane/bending/shear distinction is made when choosing the values of the corresponding elastic modulus, respectively E_M, E_F and G_T. The normal forces per unit length and the bending moments per unit length are calculated using the constitutive matrix for a plane stress state. An explicit code is used for the modeling. Eq. (3) gives the values of the forces and moments at the iteration $t + \Delta t$, which are calculated from their values at the previous iteration:

$$\begin{aligned} \begin{bmatrix} N_{xx}(t+\Delta t) \\ N_{yy}(t+\Delta t) \end{bmatrix} &= \begin{bmatrix} N_{xx}(t) \\ N_{yy}(t) \end{bmatrix} + \frac{e \cdot E_M(t) \cdot \Delta t}{1-\upsilon^2} \begin{bmatrix} 1 & \upsilon \\ \upsilon & 1 \end{bmatrix} \begin{bmatrix} \dot{\varepsilon}_{xx} \\ \dot{\varepsilon}_{yy} \end{bmatrix} \\ \begin{bmatrix} M_{xx}(t+\Delta t) \\ M_{yy}(t+\Delta t) \end{bmatrix} &= \begin{bmatrix} M_{xx}(t) \\ M_{yy}(t) \end{bmatrix} + \frac{e^3 \cdot E_F(t) \cdot \Delta t}{12(1-\upsilon^2)} \begin{bmatrix} 1 & \upsilon \\ \upsilon & 1 \end{bmatrix} \begin{bmatrix} \dot{k}_{xx} \\ \dot{k}_{yy} \end{bmatrix} \\ \begin{bmatrix} Q_{xx}(t+\Delta t) \\ Q_{yy}(t+\Delta t) \end{bmatrix} &= \begin{bmatrix} Q_{xx}(t) \\ Q_{yy}(t) \end{bmatrix} + \Delta t \cdot K_y \cdot G_T(t) \cdot e \begin{bmatrix} 1 & 0 \\ 0 & 1 \end{bmatrix} \begin{bmatrix} 2\dot{\varepsilon}_{xz} \\ 2\dot{\varepsilon}_{yz} \end{bmatrix} \end{aligned} \tag{3}$$

where $\dot{\varepsilon}_{ij}$ and $\dot{k}_{ij}$ represent respectively the strain rates in membrane and bending, Q_{ij} is the transverse shear, e the thickness of the panel, υ the Poisson's ratio of the fabric and Δt the time step. The elastic modulus E_F, which represents the bending stiffness, is that of the woven composite oriented at 0/90°. The elastic modulus E_M is that of the resin and the transverse shear modulus G_T is that of the whole skin. These two moduli are given by the manufacturer of the woven fabrics. K_y is a transverse shear correction factor. It is value is set to 5/6.

Concerning in-plane shear behavior, it has been observed experimentally that pseudo-plasticity was the predominant phenomenon. Therefore, the in-plane shear forces per unit length are calculated from the in-plane shear elastic strain (4):

$$\begin{cases} N_{xy}(t) = e \cdot \Delta t \cdot G_M \cdot 2 \cdot \varepsilon^e_{xy} \\ M_{xy}(t) = \frac{e^3}{6} \cdot \Delta t \cdot G_M \cdot k^e_{xy} \end{cases} \quad \text{with} \quad \begin{cases} \varepsilon^e_{xy} = \varepsilon^t_{xy} - \varepsilon^p_{xy} \\ k^e_{xy} = k^t_{xy} - k^p_{xy} \end{cases} \tag{4}$$

where G_M is the in-plane shear modulus. It is given experimentally by a tensile test of the woven fabric oriented at ±45°. $(\varepsilon^e_{xy}, k^e_{xy})$ are the in-plane shear elastic strains, $(\varepsilon^t_{xy}, k^t_{xy}$ the in-plane shear total strains and $(\varepsilon^p_{xy}, k^p_{xy})$ the in-plane shear plastic strains. The calculation of these strains is carried out in two principal steps. Firstly, in an elastic prediction step, the strain increment is assumed to be purely elastic. Secondly Eq. (5) is used to verify the nature of the stress computed under the elastic prediction:

$$f = |\sigma_{xy}| - R - \sigma_0 \tag{5}$$

where σ_{xy} is the in-plane shear stress, σ_0 the plastic strength and R the hardening variable.

If $f > 0$, a plastic correction is carried out using a Newton–Raphson iterative scheme to find the value of the plastic strain, as defined in [20].

The micro-cracking of the resin is represented by the degradation of the 2D elements. Due to the thin nature of the skin, the damage can be assumed to be the same throughout its thickness. The evolution of the membrane, bending and transverse shear modulus due to damage is described by a single parameter (d). As developed in [21], (d) is a function of the energy release rate Y, obtained by differentiating the elastic energy W_e with respect to the damage (6):

$$\begin{aligned} E_M(t) &= (1-d) \cdot E_M \\ E_F(t) &= (1-d) \cdot E_F \\ G_T(t) &= (1-d) \cdot G_T \\ Y &= -\frac{1}{2}\frac{\partial W_e}{\partial d}; \quad d = \frac{\langle Y - Y_0 \rangle_{\geq 0}}{Y_c} \end{aligned} \tag{6}$$

where Y_0 controls the damage initiation and Y_c the damage evolution from the initiation to the failure, as defined in [22]. Classically (d) varies between 0 (no damage) and 1 (entirely damaged).

The fibers have been modeled using rod elements, which have been integrated in the formulation of the 2D specific element. A linear elastic material law with brittle failure in tension has been chosen. As shown in [23], tensile failure properties for woven fab-

ric glass/epoxy composite is highly dependent on the strain rate. Thus the strain to failure ε_r implemented increases according to the strain rate. In order to represent the behavior of the non-stabilized bundles, the compression stiffness of the rod is set to zero when the resin is totally damaged.

This element has been implemented in the F.E. explicit software RADIOSS (Altair Hyperworks) using USERS elements and USERS material laws.

3.3. Identification

The matrix modulus E_M is a material property given by the fabric's manufacturer. The other parameters are identified with a reverse engineering method which consists of minimizing the difference between experimental and computed load/displacement curves. This optimization is carried out using the numerical tool Cobyla, which is an implementation of Powell's nonlinear derivative–free constrained optimization that uses a linear approximation approach [24].

With this approach:

- quasi-static tensile tests have been performed on the woven fabric oriented at 0°/90° to determine the tensile modulus E_F. The stiffness E_{Fiber} of the rods is then deduced from E_F and E_M from the classic rules of mixture.
- the influence of the strain rate upon the strain to failure ε_r of the rods is identified with dynamic tensile tests on 0°/90° specimens.
- the parameters governing the in-plane shear behavior (G_M, σ_0 and R) have been identified by performing tensile tests on the same woven fabric oriented at ±45°.
- the evolution of the damage parameter (d) has been calculated from static and dynamic indentation tests.

The identified parameters for the modeling are given in Table 2.

4. Validation

In order to validate the strategy of modeling of the woven composite skin, three tests have been modeled: a static indentation, a low-velocity normal impact and a high-velocity oblique impact. These tests have been carried out on the same sample defined in the experimental study. The mechanical characteristics of the materials are given in Table 1. To optimize the calculation time, the developed formulation is used only in the area located below the indentor (Fig. 6).

The mesh size in the impacted region is 1 mm × 1 mm in agreement with the measured woven fabric pattern. The other part of the skin is modeled using classic composite shell elements, with an edge length varying from 1 to 20 mm. 3D elements have been used to model the 20 mm thick foam core. 7 elements are placed in the core thickness, their height varying from 1 to 5 mm. The indentor is modeled using RADIOSS spherical rigid wall, which is an undeformable solid. This modeling contains about 5000 specific shell elements, 10,000 rod elements, 6000 composite shell elements and 80,000 volume elements.

At this stage of the study, the foam core is considered as a boundary condition for the woven skin. It is modeled by a constitutive law implemented in RADIOSS which takes into account the classic behavior of this kind of foam in compression. This law is an elastoplastic law. It provides a good representation of the elastic behavior and the crushing of the foam. The densification of the foam is carried out by adding a term of pressure (P) to the stress. This pressure is dependant on the volumetric strain (7):

$$P = -\frac{P_0 \cdot \gamma}{1+\gamma-\Phi} \quad \text{with} : \gamma = \frac{V}{V_0} - 1 + \gamma_0 \tag{7}$$

where γ is the volumetric strain, Φ the porosity, P_0 the initial air pressure, γ_0 the initial volumetric strain, V the volume of the element and V_0 the initial volume of the element.

Table 2
Identified parameters for the modeling of the (7781/913).

E_{Fiber} (MPa)	40,000	G_M (MPa)	4500
E_M (MPa)	3000	σ_0 (MPa)	40
E_F (MPa)	17,000	R (MPa)	220
Y_0 (J)	10	Y_c (J)	0.1

4.1. Static validation

A static indentation test has been conducted at the velocity of 2 mm/min using a compressive testing machine. The vertical displacement of the indentor and the applied load have been acquired. The panel described above is simply supported. The specimen is indented by a 19 mm diameter sphere.

This loading has been reproduced numerically by applying an imposed displacement to a spherical rigid indentor. Fig. 7 shows the experimental and numerical curves of the load applied on the panel against the displacement of the indentor. The calculation results correspond to the test measures.

The fracture surface observed on the skin after the test is cross shaped, and follows the same orientation as the woven fibers. This cross-shape failure is clearly represented by the numerical modeling. It has the same dimensions as the one observed experimentally.

4.2. Low velocity validation

A low velocity indentation test has been conducted using a drop tower. The displacement of the impactor and the applied load have been acquired during the test. The experiments have been carried out with a 2075 g mass at a velocity of 3.1 m/s. That is to say an impact energy of 10 J. A 19 mm diameter spherical indentor has been used.

The applied loads are plotted against the displacement of the impactor. A comparison of the experimental and numerical load/displacement curves is given in Fig. 8. A good correlation between these two curves can be observed. The modeling allows an accurate reproduction of the fracture surface and of the damage size experimentally obtained.

Moreover, the skin failure load for the low velocity indentation is 44% higher than for the static indentation. The same can be seen for the failure deflection, which is 40% higher. The strain rate dependence of the tensile failure properties of the woven skin is well represented by the modeling.

4.3. High velocity oblique impact validation

The impact tests presented in the experimental analysis (Part 2) have been modeled for different values for the impact angles and velocities. The spherical impactor is defined as an underformable body which has the mass of 28 g. The initial velocity and the impact angle have been chosen in order to respect the experimental conditions.

In order to study the accuracy of the modeling, three oblique impact tests corresponding to three impact energies (57 J, 90 J and 115 J) have been modeled. The experimental and numerical fracture surfaces are shown in Fig. 9.

The three types of skin damage described in part 2 are well represented. First of all, for an impact energy of 57 J, the only damage noticed experimentally and numerically is located in the resin. The

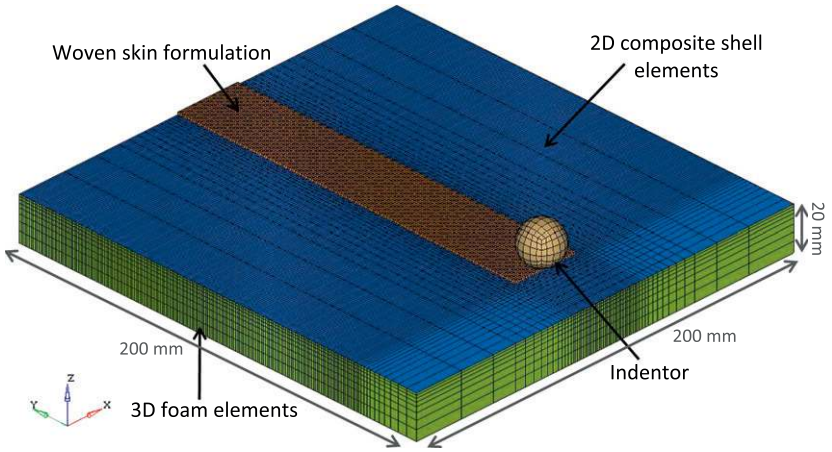

Fig. 6. Geometry of the modeling. (For interpretation of the references to color in this figure legend, the reader is referred to the web version of this article.)

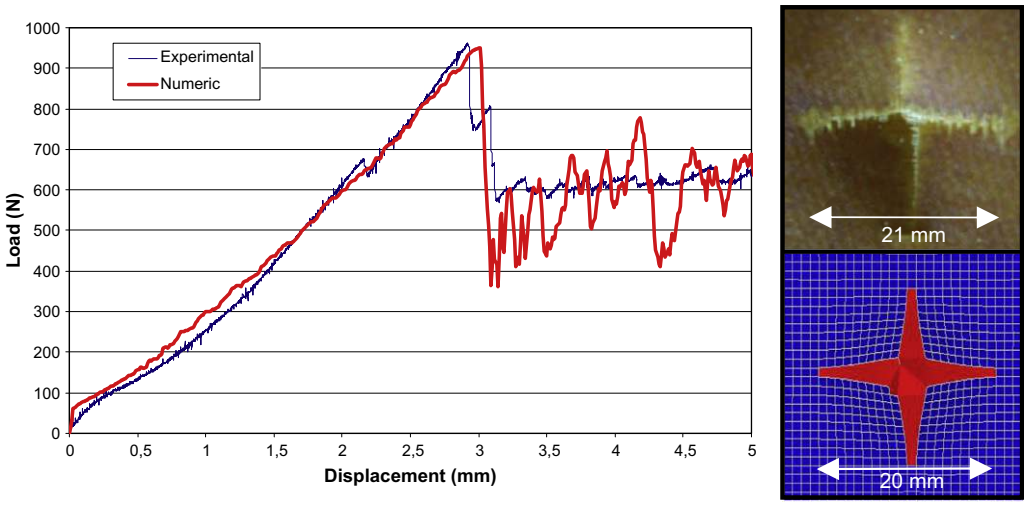

Fig. 7. Load/displacement curves for a static indentation. (For interpretation of the references to color in this figure legend, the reader is referred to the web version of this article.)

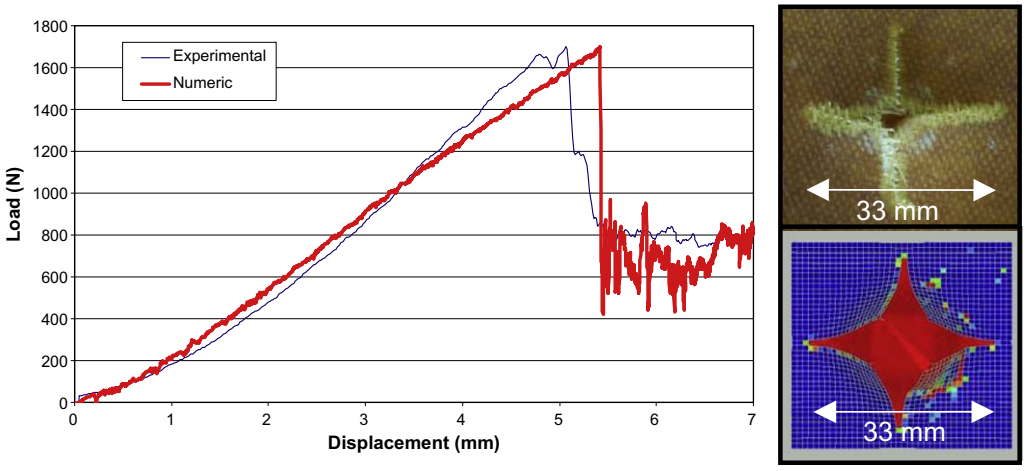

Fig. 8. Load/displacement curves for a low energy impact. (For interpretation of the references to color in this figure legend, the reader is referred to the web version of this article.)

length of the damaged area is obtained with a maximum error of 5%. Secondly, for an impact energy of 90 J, fiber breakage is observed experimentally as well as in the modeling. The longitudinal crack obtained numerically is 10% larger than the experimental one. Furthermore, the absorbed energy obtained by measuring the initial and final velocities of the steel ball, both experimentally

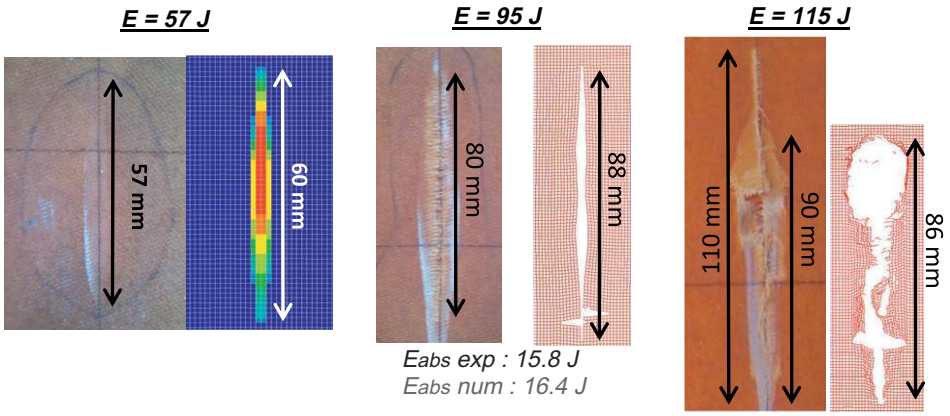

Fig. 9. Experimental and numerical fracture surfaces. (For interpretation of the references to color in this figure legend, the reader is referred to the web version of this article.)

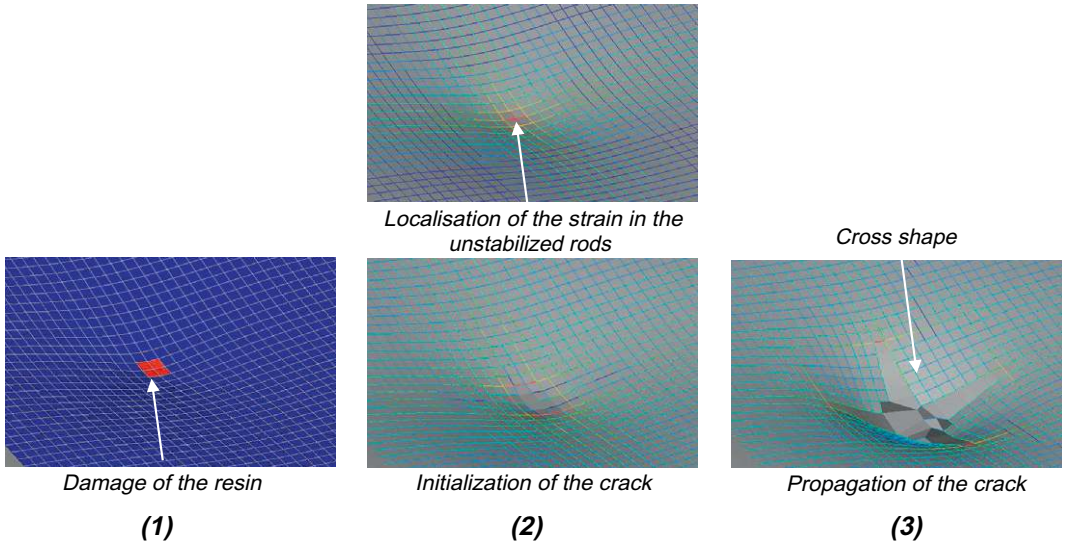

Fig. 10. Damage mechanisms for low velocity normal impacts. (For interpretation of the references to color in this figure legend, the reader is referred to the web version of this article.)

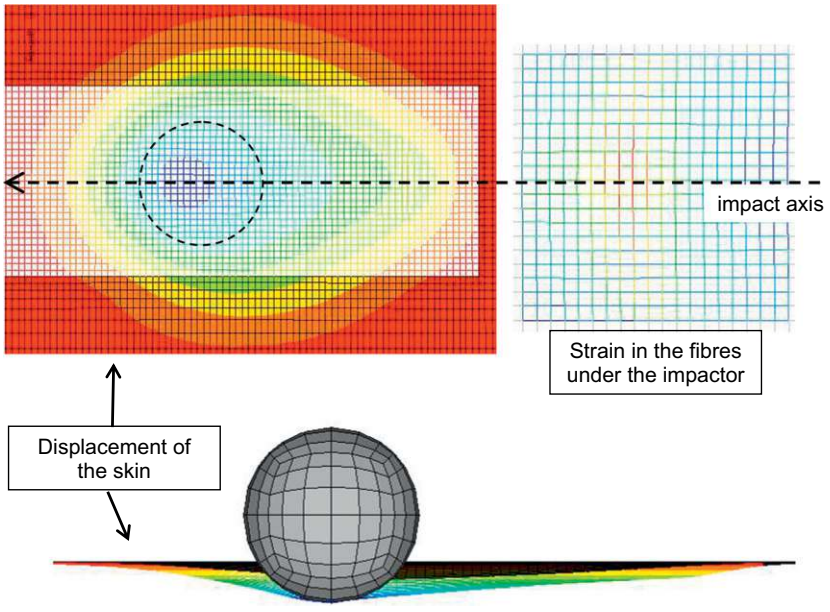

Fig. 11. Displacement of the skin and bundles strains. (For interpretation of the references to color in this figure legend, the reader is referred to the web version of this article.)

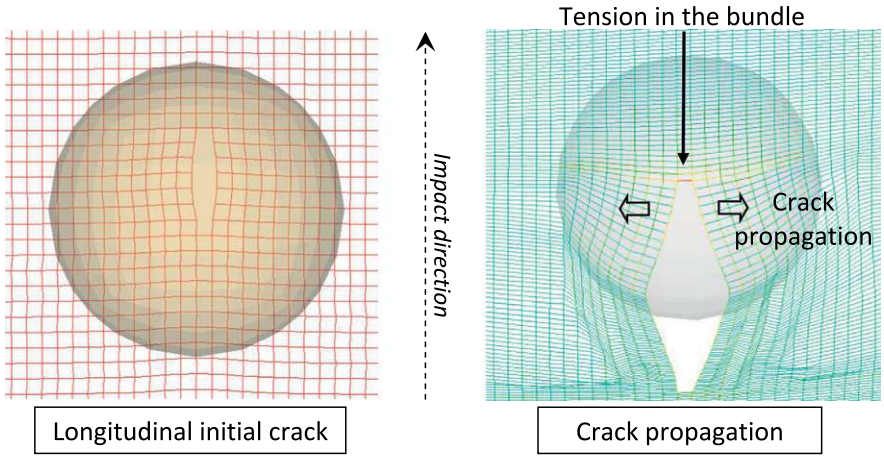

Fig. 12. Initiation and propagation of the crack. (For interpretation of the references to color in this figure legend, the reader is referred to the web version of this article.)

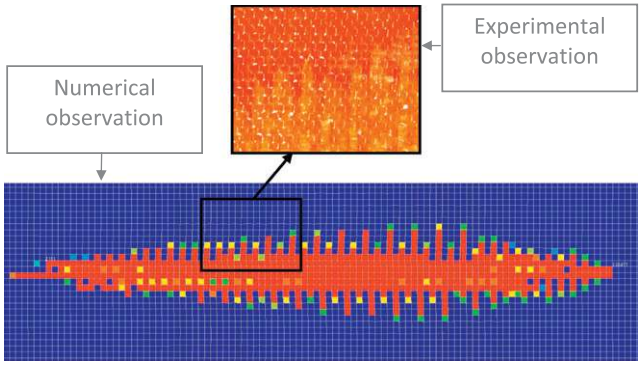

Fig. 13. Damaged area and transverse micro-cracking of the matrix. (For interpretation of the references to color in this figure legend, the reader is referred to the web version of this article.)

and numerically, is compared. A good correlation is obtained with an error of 4%. Finally, for the impact energy set to 115 J, the projectile perforates the skin. Since the contact between the table and the impactor has not been modeled, only the distance between the first breakages of bundles and the region of the perforation is compared. The error is 10%.

5. Discussion

The main difficulties in the studied tests are the insufficient amount of data recorded during the impact, and the complexity of the damage mechanisms in play in these types of impacts. Data available for the normal low velocity impact includes the impact load/displacement curves and the fracture surface. With regards to the oblique impact tests, post-mortem analysis of the impacted panels was carried out. Thus, the results given by the modeling have been analyzed in order to provide a better understanding of the normal low-velocity impact, and the high velocity oblique impact response of the woven covering.

5.1. Damage mechanisms for normal impact

The damage mechanisms for this kind of loading can be divided into three steps. Firstly the skin under the indentor is principally loaded in bending. This large load leads to the apparition of the resin failure, in a localized area under the impactor (Fig. 10-1). Secondly, the matrix being damaged, the rods located directly under the indentor carry all the loads. When the ultimate strain value

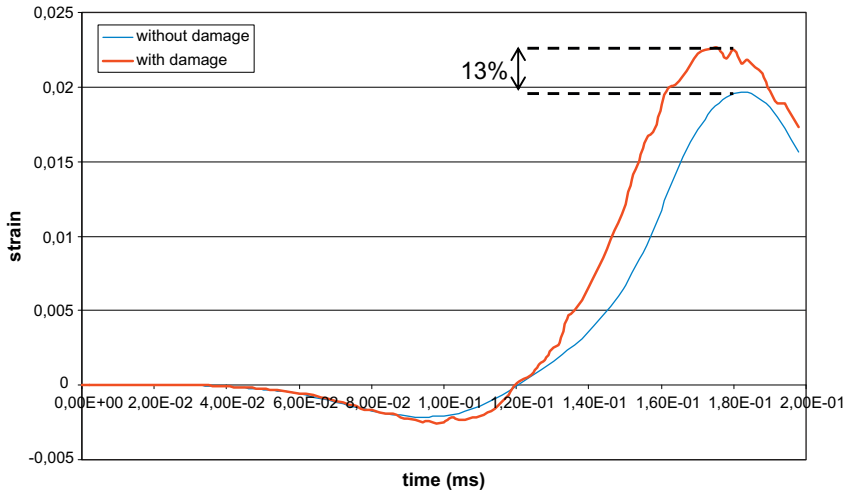

Fig. 14. Longitudinal computed strain on an impacted rod with and without taking into account resin's damage. (For interpretation of the references to color in this figure legend, the reader is referred to the web version of this article.)

is reached, the rod fails and the crack initiates (Fig. 10-2). Finally, the crack opens with a cross shape oriented in the direction of the fibers. The rods located in the end of the cracks fail successively under tension (Fig. 10-3).

5.2. Damage mechanisms for oblique impacts

The shape of the out of plane displacement of the skin is observed (Fig. 11). It reaches its maximum value directly under the impactor. Given that the foam is permanently crushed after it has been compressed by the steel ball, the skin is bent along the firing axis. Thus, the tensile strain in the fibers is greater under the projectile on the rods perpendicular to the impact axis.

When the strain on the rods reaches the tensile failure strain of the material, the crack initiates, and is oriented along the impact axis. The impactor then opens the crack whilst moving along the firing axis. The bundles in front of the crack are mainly loaded in tension. The failure of these bundles causes the crack to propagate in the direction of impact (Fig. 12), until either the ball rebounds or penetrates the skin.

Another phenomenon which can be observed numerically is the damage of the resin in the contact area. This is mainly caused by the bending of the skin (87% of the damage is due to the bending and 13% to the transverse shear). The damaged area is characterized by numerous lines of damaged resin perpendicular to the trajectory of the steel ball. This represents micro-cracking propagations in the matrix due to the local bending induced by the impactor (Fig. 13).

The consequence of the resin damage is an increase of the strain on the rods. Indeed, Fig. 14 shows the evolution of the strain versus time on the same impacted rod for two different calculations: one with the damage of the resin taken into account, and one with no matrix damage. The value of the strain on the rods is 13% higher when the matrix is damaged.

Thus, the initiation and propagation of the crack in the skin depends simultaneously on the bending stiffness of the skin, the material properties of the foam, the failure strain of the fibers and the damage of the resin.

6. Conclusion

In order to simulate the behavior of the sandwich panels submitted to oblique impacts, a semi-continuous modeling of the skin has been developed. The scale of the modeling is the woven pattern scale. The modeling strategy results from the analysis of the damage observed experimentally. A study of oblique impacts has been performed on a sandwich structure made up of a foam core and a thin woven composite skin. The impact energies have been varied from 50 J to 230 J to observe the kinematics of the damage. For the lower energies, only the resin is damaged. For greater energies, fiber breakage can lead to skin perforation.

The modeling strategy consists of separating the functions of the bundles from those of the resin. This modeling gives a good representation of the kinematics of the skin damage. It has been validated by representing several load cases: static normal indentation, low velocity normal impact and high velocity oblique impact. Calculation results correlate accurately with the experimental results. Furthermore, the analysis of the numerical results allows a more profound understanding of the mechanisms involved in the response of the woven skin. The resin's damage leads to a state of the skin where the bundles are no longer stabilized. These bundles can fail in tension. The crack grows with the successive breakage of the bundles located at the end of the crack.

Work is currently being developed in order to allow the simulation of impacts on woven skins:

- with the bundles oriented at 45° from the impact axis,
- made of two plies with different orientations.

Moreover, a study concerning the modeling of the skin/core interface and the development of a more representative material law for the foam core is being conducted.

References

[1] Petit S, Bouvet C, Bergerot A. Impact and compression after impact experimental study of a composite laminate with a cork thermal shield. Compos Sci Technol 2007;67(15–16):3286–99.
[2] Guinard S, Allix O, Guedra-degeorges D, Vinet A. A 3D damage analysis of low-velocity impacts on laminate composites. Compos Sci Technol 2002;62(4):585–9.
[3] Fuoss E, Straznicky PV, Poon C. Effect of stacking sequence on the impact resistance in composite laminates – Part 1: parametric study. Compos Struct 1998;41:67–77.
[4] Belingardi G, Vadori R. Influence of the laminate thickness in low velocity impact behavior of composite material plate. Compos Struct 2003;61:27–38.
[5] Cartie DDR, Irving PE. Effect of resin and fibre properties on impact and compression after impact performance of CFRP. Composites Part A 2002;33:486–93.
[6] Viot P, Ballere L, Guillaumat L, Lataillade JL. Scale effects on the response of composite structures under impact loading. Eng Fract Mech 2008;75:2725–36.
[7] Atas C, Sayman O. An overall view on impact response of woven fabric composite plates. Compos Struct 2008;82:336–45.
[8] Choi IH. Contact force history analysis of composite sandwich plates subjected to low-velocity impact. Compos Struct 2006.
[9] Schubel PM, Luo JJ, Daniel IM. Low velocity impact behavior of composite sandwich panels. Composites Part A 2005;36:1389–96.
[10] Schubel PM, Luo JJ, Daniel IM. Impact and post impact behavior of composite sandwich panels. Composites Part A 2007;38:1051–7.
[11] Cantwell WJ, Morton J. Comparison of the low and high velocity impact response of CFRP. Composites 1989;20:545–51.
[12] Cantwell WJ, Morton J. The influence of varying projectile mass on the impact response of CFRP. Compos Struct 1989;13:101–14.
[13] Iannucci L. Progressive failure modelling of woven carbon composite under impact. Int J Impact Eng 2006;32:1013–43.
[14] Iannucci L, Willows ML. An energy based damage mechanics approach to modeling impact onto woven composite materials: Part II. Experimental and numerical results. Composites Part A 2007;38:540–54.
[15] Duan Y, Keefe M, Bogetti TA, Powers B. Finite element modelling of transverse impact on a ballistic fabric. Int J Mech Sci 2006;48:33–43.
[16] Zhou G, Sun X, Wang Y. Multi-chain digital element analysis in textile mechanics. Compos Sci Technol 2004;64:239–44.
[17] Bahei-el-din YA, Rajendran AM, Zikry MA. A micromechanical model for damage progression in woven composite systems. Int J Solids Struct 2004;41:2307–30.
[18] Nilakantan G, Keefe M, Bogetti TA, Adkinson R, Gillespie JW. On the finite element analysis of woven fabric impact using multiscale modeling techniques. Int J Solids Struct 2010:2300–15.
[19] Belytschko T, Lin JI, Tsay CS. Explicit algorithms for the nonlinear dynamics of shells. Comput Methods Appl Mech Eng 1984;42:225–51.
[20] Simo J-C, Hugues TJ-R. Computational Inelasticity. Springer; 2000.
[21] Coutellier D, Rozycki P. Multi-layered multi-material finite element for crashworthiness studies. Compos Part A: Appl Sci Manuf 2000;31(8):841–51.
[22] Ladeveze P, Le dantec E. Damage modeling of the elementary ply for laminated composites. Compos Sci Technol 1992;43(3):257–67.
[23] Naik NK, Yernamma P, Thoram NM, Gadipatri R, Kavala VR. High strain rate tensile behavior of woven fabric E-glass/epoxy composite. Polym Test 2010;29:14–22.
[24] Powell MJD. A direct search optimization method that models the objective and constraint functions by linear interpolation. Adv Optim Numer Anal 1994:51–67.